ACADÉMIE
DES SCIENCES
INSTITUT DE FRANCE

Comptes Rendus
Physique

Yann Balland and Franck Pereira dos Santos

Measuring short range stray electric fields with a force quantum sensor

Volume 26 (2025), p. 631-640

Online since: 2 October 2025

https://doi.org/10.5802/crphys.264

The Comptes Rendus. Physique *are a member of the Mersenne Center for open scientific publishing*
www.centre-mersenne.org — e-ISSN : 1878-1535

ACADÉMIE DES SCIENCES
INSTITUT DE FRANCE

Comptes Rendus. Physique
2025, Vol. 26, p. 631-640
https://doi.org/10.5802/crphys.264

Research article / *Article de recherche*

Measuring short range stray electric fields with a force quantum sensor

Mesures de champs électriques parasites à courte distance à l'aide d'un capteur quantique de force

Yann Balland [a] **and Franck Pereira dos Santos** [*, a]

[a] LTE, Observatoire de Paris, Université PSL, Sorbonne Université, Université de Lille, LNE, CNRS, 61 avenue de l'Observatoire, 75014 Paris, France

E-mail: franck.pereira@obspm.fr (F. Pereira dos Santos)

Abstract. We use a quantum sensor based on trapped atom interferometry, and designed for probing short range atom-surface interactions, to characterize parasitic electric fields produced by adsorbed atoms or surface charges on a dielectric mirror. Applying controlled external fields with in-situ electrodes allows measuring electric field gradients with a relative uncertainty of order of 1% via variations of the force induced onto the atoms. More, our sensor can also be configured as a trapped microwave clock, allowing for direct measurements of the electric field amplitude via the Stark shift of the hyperfine transition frequency. Such measurements of the electric field amplitudes and gradients as a function of the atom-surface distance can be used to construct a model for the spatial distribution of the atoms adsorbed onto the surface of the mirror, and to accurately correct local force measurements, such as related to the Casimir–Polder interaction, from the detrimental impact of adsorbed atoms or stray charges.

Résumé. Nous utilisons un capteur quantique basé sur l'interférométrie à atomes piégés, et conçu pour sonder les interactions atomes-surface à courte distance, pour caractériser les champs électriques parasites produits par des atomes adsorbés ou des charges de surface sur un miroir diélectrique. L'application à l'aide d'électrodes in situ de champs externes contrôlés permet de mesurer les gradients de champ électrique avec une incertitude relative de l'ordre de 1 % grâce aux variations de la force induite sur les atomes. En outre, notre capteur peut également être configuré comme une horloge micro-onde piégée, ce qui permet de mesurer directement l'amplitude du champ électrique par le biais du décalage Stark de la fréquence de la transition hyperfine. Ces mesures des amplitudes et des gradients du champ électrique en fonction de la distance atomes-surface peuvent être utilisées pour construire un modèle de distribution spatiale des atomes adsorbés sur la surface du miroir et pour corriger avec précision les mesures de force locale, telles que celles liées à l'interaction Casimir–Polder, de l'impact préjudiciable d'atomes adsorbés ou de charges parasites.

Keywords. Quantum sensing, Short range forces, Electric fields.

Mots-clés. Capteurs quantiques, Forces à faible distance, Champs électriques.

Funding. European Union's Horizon 2020 Research and Innovation Programme, Agence Nationale de la Recherche (grant no. ANR-18-QUAN0015-01).
Note. Article submitted by invitation.

Manuscript received 18 May 2025, revised 11 August 2025, accepted 17 September 2025.

* Corresponding author

1. Introduction

Quantum sensors based on atom interferometry allow for performing measurements of inertial forces [1] with excellent stabilities and accuracies. They now find applications in a variety of domains, such as geoscience, on the ground [2], onboard ships and planes [3,4] or in space [5–9], inertial navigation [10], fundamental physics [11–14] and metrology [15]. In particular, instruments based on free falling atoms have reached a level of maturity that allowed for their transfer to the industry, the development of first commercial sensors [16] that have been successfully deployed on the field [17–19], despite their relatively large size and power consumption. Instruments based on trapped architectures, on the other hand, despite being less advanced, promise much greater compactness, which motivates intense research efforts to further push their performance [20,21]. Key challenges in this domain are the preservation of the atomic coherence despite their trapping [22–26], and the coping with new systematics, originating from the architecture of the sensor itself [27] or from its environment [28,29], such as the proximity of a substrate for atom chips for instance. Motivated by the potential of this technology, we have developed a trapped atom sensor aiming at performing local force measurements [30], and we have recently shown its ability to resolve tiny short range forces, with unprecedented stabilities in the quectoNewton range, such as the Casimir–Polder force between the atoms and the surface of a dielectric mirror [31]. As already demonstrated in [29,32,33], such measurements are prone to systematics related to atoms being adsorbed onto the surface or to stray charges, that produce parasitic forces originating from electric field gradients. In [31], their effect was evaluated with an empirical model, based on measurements of the force at large distances. Instead, we show in this article that our platform can be used to directly measure locally the electric field in the vicinity of the surface, with electric field gradients measured with our force sensor, and electric fields determined via hyperfine clock measurements. This allows for the characterisation of the distribution of adsorbed atoms and eventually charges onto the surface, and for the correction of force measurements from their detrimental impact.

2. Principle of the force sensor

We briefly recall here the principle of our force sensor, previously detailed in [31]. A sample of ultracold 87Rb atoms produced in a lower vacuum chamber via evaporative cooling in a crossed dipole trap is first transported with a Bloch elevator close to the surface of a dielectric mirror located inside an upper chamber. It gets recaptured in a shallow vertical optical lattice, produced by a 532 nm laser retroreflected on the surface of the mirror, with an additional transverse confinement provided by a progressive wave infrared laser at 1064 nm. After 500 ms trapping time, we are left with a maximum number of 1000 atoms prepared in the $F = 1$, $m_F = 0$ state, with rms sizes of 3.5 μm along the vertical direction and 50 μm in the transverse directions. Wannier Stark states $|W_m\rangle$, where m is the well index, are quasi-eigenstates of the system, which form a ladder of states localized around the different wells. The energy difference between adjacent Wannier Stark states is given by $\delta E = E_{m+1} - E_m = h\nu_B$, where $\nu_B = m_{Rb} g\lambda/2h$ is the Bloch frequency, m_{Rb} is the mass of a Rb atom, and λ is the wavelength of the lattice laser. Transitions between distinct Wannier Stark states in different hyperfine states, separated by Δm lattice wells, are then induced using Raman transitions between the two hyperfine ground states. In particular, a sequence of two $\pi/2$ Raman pulses, separated by a free evolution time T, realizes a Ramsey interferometer. Finally, the populations in the two output ports of the interferometer are measured with a state selective fluorescence detection on a CCD camera.

Figure 1 shows Ramsey fringe patterns obtained by scanning the frequency difference between the two Raman lasers $\Delta\nu_R$ across the $\Delta_m = +6$ transition, for two different atom-mirror distances,

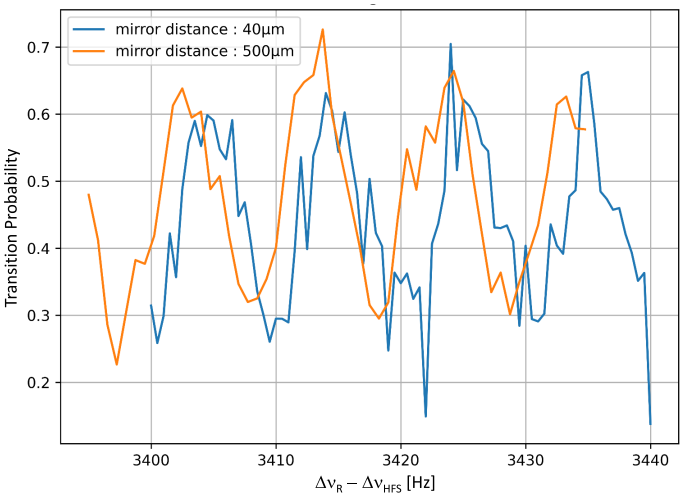

Figure 1. Ramsey fringes at two different distances, of 40 and 500 µm.

of 40 and 500 µm. The measurement parameters are a free evolution time of $T = 80$ ms, a duration of Raman pulses of $\tau = 10$ ms and a number of detected atoms of about 1000. The central fringe is located at $\Delta\nu_R = \Delta\nu_{HFS} + \Delta m\nu_B$, with $\Delta\nu_{HFS}$ the hyperfine frequency difference, which corresponds to the fringe being slightly above 3410 Hz. A clear frequency shift of the fringes of about 1.5 Hz is observed in between the two positions. If attributed solely to a change in the force, this would correspond to a shift of 0.25 Hz in the Bloch frequency and 6×10^{-28} N in the force.

For the measurements presented below, the frequency of the central fringe is actually measured using a standard mid-fringe lock method. Interleaving measurements with $\pm\Delta_m$ allows separating $\Delta\nu_{HFS}$, as well as all other clock-type contributions and their fluctuations, from the force $\Delta m\nu_B$. With a free separation time of $T = 150$ ms, our sensor reaches a best short term sensitivity on the force measurement of 3.4×10^{-28} N at 1 s, and averages down to 4 qN (1 quectoNewton (qN) = 10^{-30} N) after 5 h of averaging time [31].

Figure 2 displays the results of repeated force measurements sessions, with the force determined out of interleaved $\Delta_m = \pm 6$ measurements, as a function of the atom-surface separation distance, each measurement session being performed over a few days.

The force displays measurable amplitudes at relatively large range, much larger than the 10 µm range where the stability of our sensor would allow resolving the expected Casimir force (displayed as a brown continuous line). This behaviour is attributed to parasitic forces due to electric field gradients produced by atoms adsorbed on the surface, as already demonstrated in [32,33]. Figure 2 also shows that this force evolves from one session to another, indicating that the number and/or the spatial distribution of the adsorbed atoms evolves with time. Note also that this evolution is not monotonous with time. This is related to changes in the status of the experiment in between two consecutive measurement sessions, being either off or active, but eventually performing other kinds of measurements, with different measurement cycles. We actually observed after a cold start that the force increases over a few days before reaching a steady state when the experiment performs continuously the same experimental cycle over and over. But, the force is found to slowly reduce with a time constant of order of months when letting it off in between measurements separated by weeks.

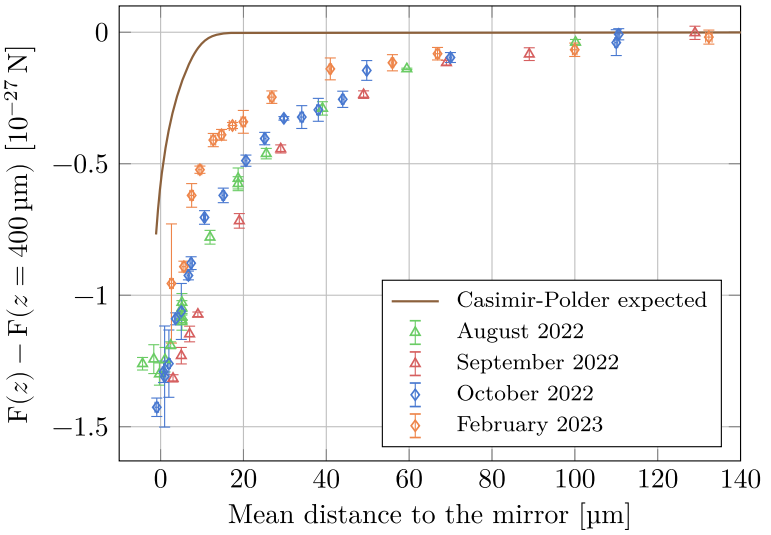

Figure 2. Force as a function of the atom-surface distance, measured over 4 measurement campaigns spanning across months.

3. Measuring electric field gradients

Parasitic electric fields E_p produced by adsorbed atoms lead to Stark shifts of the atoms energy levels $\delta E = -(\alpha_0/2)\mathbf{E}_\mathbf{p}^2$, where α_0 is the atom static polarisability, and thus to forces due to their gradients $\mathbf{F_p} = (\alpha_0/2)\nabla\mathbf{E}_\mathbf{p}^2$ to which our sensor is sensitive. The amplitude of this force can be modified by applying an additional electric field $\mathbf{E_a}$, the force then being $\mathbf{F} = (\alpha_0/2)\nabla(\mathbf{E_p} + \mathbf{E_a})^2$. This reduces to $\mathbf{F_p} + \alpha_0 \sum_i E_{\mathrm{a},i} \nabla E_{\mathrm{p},i}$, when $\mathbf{E_a}$ is homogeneous. Thus, by measuring the force as a function of the applied field E_a along one direction i, one can determine the gradient of the amplitude of the parasitic field $\nabla E_{\mathrm{p},i}$ along that direction.

In order to apply such homogeneous additional fields, electrodes have been placed inside the vacuum chamber, their arrangement being depicted in Figure 3. Four longitudinal linear rods along an horizontal direction x, placed at equal distances from the atoms, and two circular ones allow to produce electric fields aligned respectively in the (y,z) plane and along x. In particular, applying a difference of potential of $V = 1.25$ kV between the upper and lower pairs of rods allow to produce a vertical electric field of 30 kV/m, with a good homogeneity at the atoms position.

Figure 4 displays the measurements by our sensor of the force experienced by the atoms as a function of the electric field applied in the vertical direction, for two different atom-surface distances of 30 and 50 µm. We observe as expected a linear behaviour, and a linear fit to the data allows extracting the gradient of the parasitic electric field along the vertical direction (of order of 3 kV/cm^2 at these distances) with an uncertainty of order of 20 V/cm^2.

A series of such measurements can then performed at different atom-surface distances, interleaved with measurements of the force in the absence of applied electric field. Figure 5 displays the results of a campaign of such concurrent measurements, with the measurements of the force at the top of the figure and of the electric field gradients in the middle.

It also displays, at the bottom and as crossed symbols, the reconstructed amplitudes of the electric field along the vertical direction, obtained via the integration of the gradient measurements. Finally, the force due to stray electric fields can be calculated out of the reconstructed electric field, and the results are displayed as green crosses at the top of the figure. This clearly shows that the force at large distances (larger than about 20 µm) is dominated by

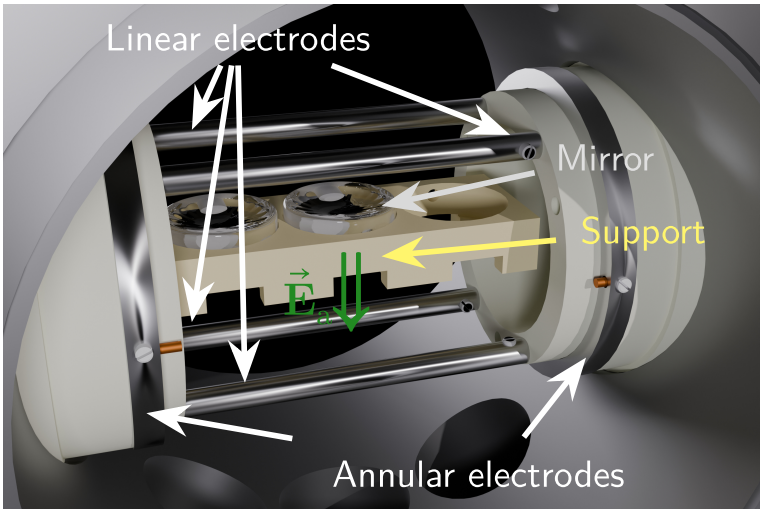

Figure 3. Arrangement of the electrodes around the mirror of interest, placed in its ceramic support, at the center of the upper vacuum chamber.

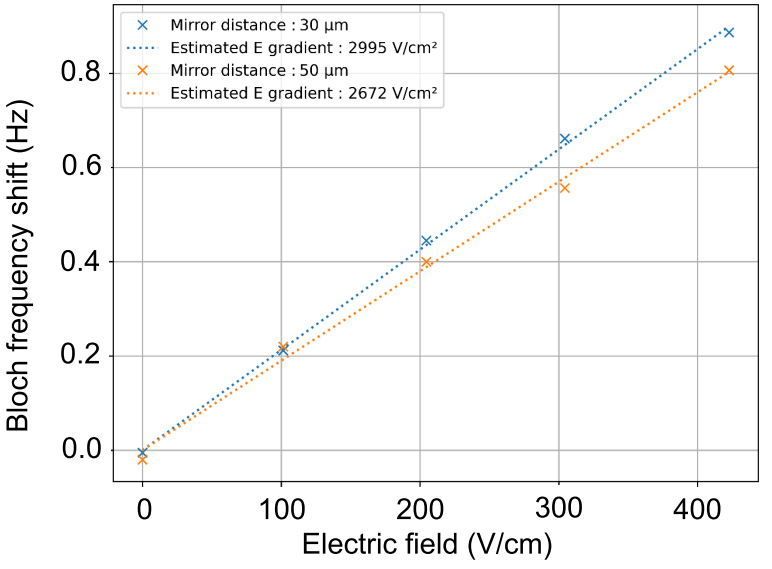

Figure 4. Force versus applied electric field, for two different atom-surface distances.

the effect of stray electric fields. As for the deviation at the shortest distance between the direct force measurements and the force due to stray electric fields, it is related to the Casimir–Polder force [31]. Note that differential measurements are displayed in all plots, the figures displaying the difference in the force, the gradient and the electric field with respect to reference values obtained very far from the surface, at a distance of about 400 µm.

4. Model of the adsorbed atom distribution

Similar to what was performed in [33], and more recently in [31], we first tried to reproduce the dependence of the bare force measurements (i.e. with no applied electric field) as a function of

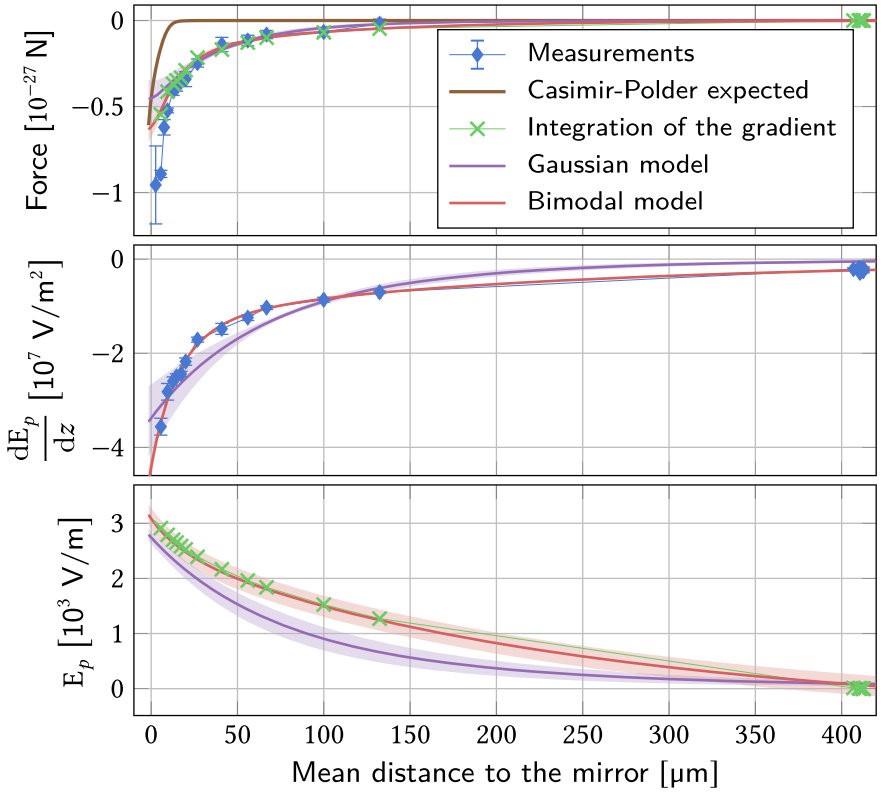

Figure 5. Measurements and models of the force (top) and the electric field gradients (middle) as a function of the atom-surface distance, and the corresponding reconstructed electric field (bottom). Measurements are displayed by symbols, and models by continuous lines. Shaded areas represent the uncertainties in the models. The measurements are displayed as differential, taking the measurement at the largest distance of about 400 μm as a reference.

the distance by a model of the effect of adsorbed atoms, with a Gaussian density distribution at the surface with a rms width of the order of the transverse size of the atomic sample in the trap. The results of such a model is displayed on Figure 5 as a purple line. While this model captures reasonably well the dependence of the bare force, it fails reproducing the measured electric field gradients, as shown in Figure 5, middle.

A better agreement is found by modelling the adsorbed atom distribution by a bimodal double gaussian distribution, one gaussian distribution function having a transverse size of 31(3) μm, of the order of the atomic sample, and the second one having a much larger size, of 410(20) μm, which we attribute to adsorbed atoms that have diffused across the surface. By contrast with the first approach, we actually adjusted the model onto the measured gradients rather than the force, with four fit parameters, two rms sizes and two amplitudes, taking distributions co-centered with the atomic cloud.

The results of this last model, which is displayed in Figure 5 as a red line, allows reproducing both the measured electric field gradients and the corresponding (bare) force. We understand from this bimodal distribution that our measurements were performed at a time after starting the experiment where adsorbed atoms had started diffusing slowly across the surface, leading to a wider density distribution that may not have reached its stationary state.

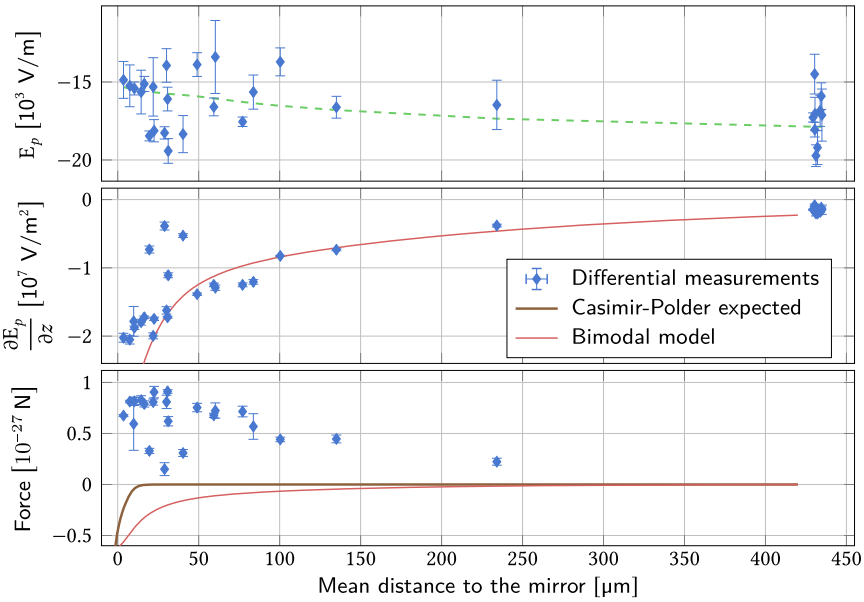

Figure 6. Concurrent measurements of the electric field, its gradient and the force versus the atom-surface distance after UV illumination of the mirror.

5. UV illimination

UV illumination was shown effective to force the desorption of atoms adsorbed onto surfaces [34–36]. This motivated us to expose the surface of the mirror to the UV light produced by 800 mW LED at 370 nm. Several sessions of illuminations over a couple hours have been performed, with differential measurements of the electric field gradients and the force at distances of 40 and 400 μm in between. While we observed no significant variations over the first sessions, a dramatic change occurred in the force after some time, which actually changed sign, while leaving the electric field gradients unchanged. Such a behaviour could be explained by the appearance of an additional electric field, with an amplitude larger than the one produced by the adsorbed atoms, but with an opposite sign. To confirm this hypothesis, we have performed direct measurements of the electric field, via clock-type measurements of the differential Stark shift of the hyperfine transition $(\delta\alpha_0/2)|E|^2$. For that, we performed Ramsey spectroscopy of that transition, using a sequence of two $\pi/2$ microwave pulses separated by a free evolution time of 300 ms. We then measure the position of the central fringe of the Ramsey fringe pattern, which is shifted in the presence of stray electric field shift. To amplify the effect of the field E_p we want to determine [37], we added an applied field E_a of 30 kV/m and performed measurements with alternated signs $\pm E_\mathrm{a}$. The corresponding difference between the differential Stark shifts in the two different orientations of the applied field is then given by $2\Delta\alpha_0 E_\mathrm{p} E_\mathrm{a}$. This differential measurement allows for separating this quantity from all other shifts of the hyperfine transition. Finally, this method allows us to determine the electric field with an uncertainty of order of 300 V/m for half an hour averaging time.

The results of these measurements, concurrent with electric field gradients and force measurements are displayed on Figure 6. One sees at the bottom of the figure that the force indeed changed sign with respect to before UV illumination. More, we clearly observe the presence of a large electric field of order of −15, −20 kV/m, rather constant with the atom-surface distance. We attribute this field to stray charges, created by the UV illumination, and distributed rather

homogeneously across the surface, thus inducing no significant change to the gradient. Finally, the UV illumination turned out to be detrimental, resulting in a long-standing charging of the surface, the force remaining repulsive over the following months.

Similar charging effects have actually already been observed with semiconducting or dielectric surfaces (see for instance [32,38]) and more recently in the context of electrometry with Rydberg atoms, where lasers in the blue and green spectral regions were shown to induce surface charging in glass cells filled with hot alkali vapours [39,40].

6. Conclusion

We have used a highly sensitive local force sensor to measure forces exerted onto atoms close to the surface of a mirror by adsorbed atoms that generate electric field gradients. Applying external fields with electrodes allows measuring electric field gradients via force measurements, and even electric fields directly via microwave clock measurements. These measurements allow to build models of the distribution of parasitic sources of electric fields, being either adsorbed atoms or charges. For a more complete picture though, 3D measurements, rather the 1D measurement performed here, would need to be performed, which can be done in our setup by applying external fields along all three directions. The complete knowledge of the electric gradients can then be exploited to accurately correct local force measurements from their detrimental effects, and will be instrumental for improving the measurement of the Casimir–Polder force [31], and for performing tests of gravity at short range [41] and of dark energy theories [11,12,42].

Acknowledgements

We thank Xiaobing Deng and Luc Absil for early contributions. This research has been carried out in the frame of the QuantERA project TAIOL, funded by the European Union's Horizon 2020 Research and Innovation Programme and the Agence Nationale de la Recherche (ANR-18-QUAN0015-01).

Declaration of interests

The authors do not work for, advise, own shares in, or receive funds from any organization that could benefit from this article, and have declared no affiliations other than their research organizations.

References

[1] R. Geiger, A. Landragin, S. Merlet and F. Pereira Dos Santos, "High-accuracy inertial measurements with cold-atom sensors", *AVS Quant. Sci.* **2** (2020), no. 2, article no. 024702.

[2] B. Stray, A. Lamb, A. Kaushik, et al., "Quantum sensing for gravity cartography", *Nature* **602** (2022), no. 7898, pp. 590–594.

[3] Y. Bidel, N. Zahzam, C. Blanchard, A. Bonnin, M. Cadoret, A. Bresson, D. Rouxel and M. F. Lequentrec-Lalancette, "Absolute marine gravimetry with matter-wave interferometry", *Nat. Commun.* **9** (2018), article no. 627.

[4] Y. Bidel, N. Zahzam, A. Bresson, C. Blanchard, M. Cadoret, A. V. Olesen and R. Forsberg, "Absolute airborne gravimetry with a cold atom sensor", *J. Geodesy* **94** (2020), no. 2, article no. 20.

[5] O. Carraz, C. Siemes, L. Massotti, R. Haagmans and P. Silvestrin, "A spaceborne gravity gradiometer concept based on cold atom interferometers for measuring Earth's gravity field", *Microgravity Sci. Technol.* **26** (2014), article no. 139.

[6] F. Migliaccio, M. Reguzzoni, K. Batsukh, et al., "MOCASS: a satellite mission concept using cold atom interferometry for measuring the Earth gravity field", *Surv. Geophys.* **40** (2019), no. 5, pp. 1029–1053.

[7] T. Lévèque, C. Fallet, M. Mandea, et al., "Gravity field mapping using laser-coupled quantum accelerometers in space", *J. Geodesy* **95** (2021), no. 1, article no. 15.

[8] A. HosseiniArani, M. Schilling, Q. Beaufils, et al., "Advances in atom interferometry and their impacts on the performance of quantum accelerometers on-board future satellite gravity missions", *Adv. Space Res.* **74** (2024), no. 7, pp. 3186–3200.

[9] P. Zingerle, T. Gruber, R. Pail and I. Daras, "Constellation design and performance of future quantum satellite gravity missions", *Earth Planets Space* **76** (2024), no. 1, article no. 101.

[10] Q. d'Armagnac de Castanet, C. Des Cognets, R. Arguel, et al., "Atom interferometry at arbitrary orientations and rotation rates", *Nat. Commun.* **15** (2024), no. 1, article no. 6406.

[11] M. Jaffe, P. Haslinger, V. Xu, P. Hamilton, A. Upadhye, B. Elder, J. Khoury and H. Müller, "Testing sub-gravitational forces on atoms from a miniature in-vacuum source mass", *Nat. Phys.* **13** (2017), no. 10, pp. 938–942.

[12] D. O. Sabulsky, I. Dutta, E. A. Hinds, B. Elder, C. Burrage and E. J. Copeland, "Experiment to detect dark energy forces using atom interferometry", *Phys. Rev. Lett.* **123** (2019), no. 6, article no. 061102.

[13] G. M. Tino, "Testing gravity with cold atom interferometry: results and prospects", *Quant. Sci. Technol.* **6** (2021), no. 2, article no. 024014.

[14] C. Struckmann, R. Corgier, S. Loriani, et al., "Platform and environment requirements of a satellite quantum test of the weak equivalence principle at the 10^{-17} level", *Phys. Rev. D* **109** (2024), no. 6, article no. 064010.

[15] M. Thomas, D. Ziane, P. Pinot, et al., "A determination of the Planck constant using the LNE Kibble balance in air", *Metrologia* **54** (2017), no. 4, pp. 468–480.

[16] V. Ménoret, P. Vermeulen, N. Le Moigne, S. Bonvalot, P. Bouyer, A. Landragin and B. Desruelle, "Gravity measurements below 109 g with a transportable absolute quantum gravimeter", *Sci. Rep.* **8** (2018), no. 1, article no. 12300.

[17] L. Antoni-Micollier, D. Carbone, V. Ménoret, et al., "Detecting volcano-related underground mass changes with a quantum gravimeter", *Geophys. Res. Lett.* **49** (2022), no. 13, article no. e2022GL097814.

[18] A. Güntner, M. Reich, J. Glässel, A. Reinhold and H. Wziontek, "Mobile field measurements with a quantum gravimeter: technical setup and performance", *IEEE Instrum. Meas. Mag.* **27** (2024), no. 6, pp. 53–59.

[19] M. Diament, G. Lion, G. Pajot-Métivier, S. Merlet and S. Déroussi, "The AQG-B absolute quantum gravimeter: a promising sensor for volcano monitoring", *IEEE Instrum. Meas. Mag.* **27** (2024), no. 6, pp. 17–23.

[20] M. Keil, O. Amit, S. Zhou, D. Groswasser, Y. Japha and R. Folman, "Fifteen years of cold matter on the atom chip: promise, realizations, and prospects", *J. Mod. Opt.* **63** (2016), no. 18, pp. 1840–1885.

[21] C. L. Garrido Alzar, "Compact chip-scale guided cold atom gyrometers for inertial navigation: enabling technologies and design study", *AVS Quant. Sci.* **1** (2019), no. 1, article no. 014702.

[22] G. D. McDonald, H. Keal, P. A. Altin, et al., "Optically guided linear Mach–Zehnder atom interferometer", *Phys. Rev. A* **87** (2013), article no. 013632.

[23] M. Egorov, R. P. Anderson, V. Ivannikov, B. Opanchuk, P. Drummond, B. V. Hall and A. I. Sidorov, "Long-lived periodic revivals of coherence in an interacting Bose–Einstein condensate", *Phys. Rev. A* **84** (2011), no. 2, article no. 021605.

[24] A. Hilico, C. Solaro, M.-K. Zhou, M. Lopez and F. Pereira dos Santos, "Contrast decay in a trapped-atom interferometer", *Phys. Rev. A* **91** (2015), article no. 053616.

[25] M. Ammar, M. Dupont-Nivet, L. Huet, et al., "Symmetric microwave potentials for interferometry with thermal atoms on a chip", *Phys. Rev. A* **91** (2015), no. 5, article no. 053623.

[26] C. D. Panda, M. Tao, J. Egelhoff, M. Ceja, V. Xu and H. Müller, "Coherence limits in lattice atom interferometry at the one-minute scale", *Nat. Phys.* **20** (2024), no. 8, pp. 1234–1239.

[27] B. Pelle, A. Hilico, G. Tackmann, Q. Beaufils and F. Pereira dos Santos, "State-labeling Wannier–Stark atomic interferometers", *Phys. Rev. A* **87** (2013), no. 2, article no. 023601.

[28] P. Haslinger, M. Jaffe, V. Xu, O. Schwartz, M. Sonnleitner, M. Ritsch-Marte, H. Ritsch and H. Müller, "Attractive force on atoms due to blackbody radiation", *Nat. Phys.* **14** (2018), no. 3, pp. 257–260.

[29] D. M. Harber, J. M. Obrecht, J. M. McGuirk and E. A. Cornell, "Measurement of the Casimir–Polder force through center-of-mass oscillations of a Bose–Einstein condensate", *Phys. Rev. A* **72** (2005), no. 3, article no. 033610.

[30] X. Alauze, A. Bonnin, C. Solaro and F. P. D. Santos, "A trapped ultracold atom force sensor with a m-scale spatial resolution", *New J. Phys.* **20** (2018), no. 8, article no. 083014.

[31] Y. Balland, L. Absil and F. Pereira Dos Santos, "Quectonewton local force sensor", *Phys. Rev. Lett.* **133** (2024), no. 11, article no. 113403.

[32] J. M. McGuirk, D. M. Harber, J. M. Obrecht and E. A. Cornell, "Alkali–metal adsorbate polarization on conducting and insulating surfaces probed with Bose–Einstein condensates", *Phys. Rev. A* **69** (2004), no. 6, article no. 062905.

[33] J. M. Obrecht, R. J. Wild and E. A. Cornell, "Measuring electric fields from surface contaminants with neutral atoms", *Phys. Rev. A* **75** (2007), no. 6, article no. 062903.

[34] M. Meucci, E. Mariotti, P. Bicchi, C. Marinelli and L. Moi, "Light-induced atom desorption", *Europhys. Lett.* **25** (1994), no. 9, article no. 639.

[35] L. Torralbo-Campo, G. D. Bruce, G. Smirne and D. Cassettari, "Light-induced atomic desorption in a compact system for ultracold atoms", *Sci. Rep.* **5** (2015), no. 1, article no. 14729.

[36] C. Klempt, T. van Zoest, T. Henninger, O. Topic, E. Rasel, W. Ertmer and J. Arlt, "Ultraviolet light-induced atom desorption for large rubidium and potassium magneto-optical traps", *Phys. Rev. A* **73** (2006), no. 1, article no. 013410.

[37] J. Lodewyck, M. Zawada, L. Lorini, M. Gurov and P. Lemonde, "Observation and cancellation of the dc Stark shift in strontium optical lattice clocks", *IEEE Trans. Ultrason. Ferroelectr. Freq. Control* **59** (2012), no. 3, pp. 411–415.

[38] M. Harlander, M. Brownnutt, W. Hänsel and R. Blatt, "Trapped-ion probing of light-induced charging effects on dielectrics", *New J. Phys.* **12** (2010), no. 9, article no. 093035.

[39] L. Ma, E. Paradis and G. Raithel, "DC electric fields in electrode-free glass vapor cell by photoillumination", *Opt. Express* **28** (2020), no. 3, pp. 3676–3685.

[40] L. Patrick, N. Schlossberger, D. F. Hammerland, et al., "Imaging of induced surface charge distribution effects in glass vapor cells used for Rydberg atom-based sensors", *AVS Quant. Sci.* **7** (2025), no. 2, article no. 024401.

[41] Y.-J. Chen, W. K. Tham, D. E. Krause, D. López, E. Fischbach and R. S. Decca, "Stronger limits on hypothetical Yukawa interactions in the 30–8000 nm range", *Phys. Rev. Lett.* **116** (2016), no. 22, article no. 221102.

[42] L.-L. Chen, W.-J. Xu, M.-K. Zhou and Z.-K. Hu, "Testing chameleon dark energy at short range with atom interferometer", *Phys. Rev. D* **109** (2024), no. 12, article no. 123515.